CHEMISTRY OF MATERIALS
Article

*Chem. Mater.* **2010,** *22,* 1749–1759 1749
DOI:10.1021/cm903182n

# Assemblies of Titanium Dioxide-Polystyrene Hybrid Nanoparticles for Dielectric Applications

Maxim N. Tchoul,[†] Scott P. Fillery,[†] Hilmar Koerner,[†,‡] Lawrence F. Drummy,[†,§] Folusho T. Oyerokun,[†] Peter A. Mirau,[†] Michael F. Durstock,[†] and Richard A. Vaia*[,†]

[†]*Materials and Manufacturing Directorate, Air Force Research Laboratory, AFRL/RXBN, 2941 Hobson Way, Wright-Patterson AFB, Ohio 45433,* [‡]*Universal Technology Corporation, Dayton, Ohio 45432, and* [§]*UES Inc., Dayton, Ohio 45432*

*Received October 15, 2009. Revised Manuscript Received December 14, 2009*

Macroscopic assemblies of hybrid nanoparticles composed of titanium dioxide core surrounded by covalently grafted polystyrene corona have been prepared by a combination of phosphonate coupling and "click" chemistry. The attached polymer chains existed in the brush regime, with grafting density inversely proportional to the degree of polymerization. Solution casting afforded preparation of robust films of the composite material where all the polymer chains were covalently bound to the uniformly distributed inorganic particles. Inorganic content from 60 to 80 wt % (27 to 50 vol %) was obtained by varying the molecular weight of polystyrene as well as by using the mixture of high and low molecular weight polymer for grafting. The $TiO_2$ grafted with $10^5$ g/mol polystyrene had a volume fraction of nanoparticles of 27% and exhibited glass transition at 110 °C and ~100% extensibility above $T_g$. Thin films of this material had a dielectric constant of 6.4 and a dielectric loss of 0.04 at 1 kHz.

## Introduction

Future dielectric applications in electric powered vehicles and aircraft will require power sources featuring high power density (W/kg) and energy density (J/kg), along with fast discharge rate ($< 10\,\mu$s) and higher temperature durability.[1] Modern capacitor technologies can provide a good foundation for development of such power sources, where the required energy density can be achieved through incorporation of new innovative dielectric materials combining both increased dielectric strength ($> 1000$ V/$\mu$m) and high dielectric constant ($k > 3$). Current off-the-shelf capacitors are based either on polymer films, such as polypropylene and polystyrene, or on ceramics. Thermoplastic polymers exhibit a high breakdown strength and low dissipation factor, although they possess a low dielectric constant ($k = 2-4$ for most of the nonferroelectric polymers).[2] The dielectric constant is much higher for ceramic materials (up to several thousand for $BaTiO_3$);[3] however, low breakdown strength for most of the common ceramic capacitors prevents their use as high voltage power sources.

Polymer-ceramic composites hold potential for capitalizing on the advantages of both components toward producing efficient energy storage systems. Hence, it is not surprising that the dielectric properties of these composites are being actively investigated.[4] Recent studies show that incorporation of high $k$ nanofillers, such as barium titanate,[5,6] titanium dioxide,[7,8] zirconia,[9] and alumina,[10] into a polymeric matrix can result in a moderate increase in dielectric permittivity. For instance, in the work of Badheka,[5] incorporation of 40 vol % of the 240 nm size $BaTiO_3$ nanoparticles in polystyrene increased the dielectric constant of the material from 2.6 to 20, which is a significant improvement, but is much lower than $k > 1000$ expected for barium titanate of the corresponding grain size.[11] Jylha and Sihova predicted theoretically[12] that the effective dielectric permittivity of the particle-filled composite will not increase substantially for the fractions of the filler below 30−50 vol %. This study suggests that in order to utilize the full potential of high $k$ nanofillers, a very high content of inorganic fraction is needed. Additionally, other studies have indicated that increased permittivity[13] or breakdown strength[14] may arise

*Corresponding author e-mail: richard.vaia@wpafb.af.mil.

(1) Brandstetter, S. S.; Drummy, L. F.; Tchoul, M.; Fillery, S.; Horeath, J. C.; Schweickart, D. L.; Durstock, M.; Vaia, R. A. Abstracts of Papers, 237th ACS National Meeting, Salt Lake City, UT, United States, March 22−26, 2009, Salt Lake City, UT, Salt Lake City, UT, 2009.
(2) *Handbook of Low and High Dielectric Constant Materials and Their Applications*; Academic Press: New York, 1999; Vol. *2*.
(3) Arlt, G.; Hennings, D.; de Witt, G. *J. Appl. Phys.* **1985**, *58*, 1619.
(4) Lu, J.; Wong, C. P. *IEEE Trans. Dielectr. Electr. Insul.* **2008**, *15*, 1322.
(5) Badheka, P.; Magadala, V.; Devaradju, N. G.; Lee, B. I.; Kim, E. S. *J. Appl. Polym. Sci.* **2005**, *99*, 2815.
(6) Kim, P.; Jones, S. C.; Hotchkiss, P. J.; Haddock, J. N.; Kippelen, B. M.; Seth, R.; Perry, J. W. *Adv. Mater.* **2007**, *19*, 1001.
(7) Nelson, J. K.; Forthergill, J. C. *Nanotechnology* **2004**, *15*, 586.
(8) Maliakal, A.; Katz, H.; Cotts, P. M.; Subramoney, S.; Mirau, P. *J. Am. Chem. Soc.* **2005**, *127*, 14655.
(9) Chu, B.; Lin, M.; Neese, B.; Zhang, Q. *J. Appl. Phys.* **2009**, *105*, 014103.
(10) Xu, J.; Wong, C. P. *Composites, Part A* **2006**, *38A*, 13–19.
(11) Cho, S.; Lee, J.; Hyun, J.; Paik, K. *Mater. Sci. Eng., B* **2004**, *110*, 233.
(12) Jylha, L.; Sihvola, A. *J. Phys. D: Appl. Phys.* **2007**, *40*, 4966.
(13) (a) Lewis, T. J. *Appl. Phys.* **2005**, *38*, 202. (b) Roy, M.; Nelson, J. K.; MacCrone, R. K.; Schadler, L. S. *IEEE Trans Dielectr. Electr. Insul.* **2005**, *12*, 629.
(14) Smith, R. C.; Liang, C.; Landry, M.; Nelson, J. K.; Schadler, L. S. *IEEE Trans. Dielectr. Electr. Insul.* **2008**, *15*, 187.


Published on Web 01/14/2010

in nanocomposites due to the increased fraction of the interfacial area. Considering these factors, the study of dielectric properties of hybrid polymer-ceramic nanocomposites with high content of the inorganic nanoparticles becomes tremendously interesting.

Preparation of a high inorganic content composite by conventional blending of the two components will inevitably raise the issues of inhomogeneity and aggregation. The problem can be effectively overcome by grafting the filler particles with polymer chains that are identical in molecular weight and chemical composition to the host matrix.[15] The improved wettability of the functionalized particles facilitates their homogeneous dispersion. The volume fraction of the filler particles can be maximized by reducing the fraction of host polymeric chains or completely eliminating the host matrix. The latter will ultimately lead to a composite where the entire polymeric fraction is chemically bound to the filler. At this point, the ratio between the components can be controlled by changing molecular weight or grafting density of the attached polymer. At the same time, precise tuning of the nanoparticle arrangement, particle−particle spacing, and the thermoplastic properties of the corona and the resultant assembly becomes possible through the control of molecular weight and grafting density of the polymer in the corona.

In the present work, precisely this strategy was adopted for synthesizing hybrid materials "from the bottom up". Using the previously developed "click" grafting technique,[16,17] $TiO_2$-polystyrene hybrid nanoparticles were synthesized through the reaction of the alkyne end groups of polystyrene with azides preseeded on the surface of titania. Here, we are particularly focusing on engineering of the corona in order to understand the impact of the molecular weight of the polymer on grafting density and volume fractions of the components as well as on morphology and physical properties of the resultant composite materials.

## Experimental Section

**Materials.** Titanium dioxide ($TiO_2$) nanoparticles, batch # TTO-51N, were obtained from Ishihara Sangyo Kaisha, LTD, Osaka, Japan. According to transmission electron microscopy, the particles were of rodlike shape, 18 nm in diameter and 40−50 nm in length. *N*,*N*′-Dimethylformamide (DMF) was obtained from Fisher Scientific. All other chemicals and solvents were obtained from Aldrich and Fisher Scientific. Deionized water (18 MΩcm) was used for the procedures that required water.

**Instruments.** Electron micrographs of the materials were taken on a Philips CM200 transmission electron microscope from FEI Company operating at 200 kV and on a LVEM5 transmission electron microscope from Delong Instruments operating at a nominal accelerating voltage of 5 kV. Films were microtomed to 75 nm thickness at room temperature using a RMC PowerTome. Individual particles were deposited from solutions on ∼15 nm thick amorphous carbon. For the discrete Fourier transform analysis, a 1.25 × 1.25 $\mu$m area of the image was processed using the FFT algorithm of the Image J software, followed by the azimuthal integration of the intensity. Wide angle X-ray experiments were carried out on a Statton box camera at varying sample to image plate distances in transmission mode using $CuK_\alpha$ generated by a Rigaku RU200 system. Small angle X-ray experiments were carried out on a Rigaku S-MAX 3000 3 pinhole SAXS system in transmission mode at a sample to detector distance of 150 cm. $CuK_\alpha$ radiation was generated on a Rigaku Ultrax RAG system and focused via a confocal multilayer optic system. NMR spectra of the solutions were aquired at 400 MHz on a Bruker Ultrashield 400 spectrometer. Solid-state NMR spectroscopy was performed on a TecMag Apollo 5 spectrometer at 500 MHz, using magic angle sample spinning. Low speed centrifugation was performed in an Allegra X 22 centrifuge from Beckman Coulter. High-speed centrifugation was carried out in a Sorvall WX Ultra 80 centrifuge with a T-647.5 rotor and 90 mL polyallomer tubes, all from ThermoFisher Scientific. High shear mixing was performed using a T-18 Ultra-Turrax disperser from IKA operating at 10,000 rpm. Size-exclusion chromatography (SEC) was performed using a Waters 2950 HPLC pump and a set of two 7.5 × 300 mm columns, Styragel HR-4E and HR-5E, at 1 mL/min flow rate in THF. Samples were dissolved in THF at 1−2 mg/mL concentration and filtered through 0.2 $\mu$m PTFE syringe filter prior to injection. The injection volume was 0.1 mL. To detect and analyze the eluted fractions, the set of detectors from Wyatt Inc. was utilized, that included Dawn Eos 17-angle light scattering detector, ViscoStar viscosity detector, and Optilab refractive index detector. The data were processed using Astra-5 SEC software. Thermogravimetric analysis was performed in a Q5000 TGA analyzer from TA Instruments in air in the range of 20−800 °C. TGA-mass spectrometry of the functionalized titania sample heated in helium in the range of 20−300 °C at 20 °/min was performed on a Netzsch 449C TG/DTA system at the Center for Applied Energy Research, University of Kentucky, Lexington, KY. Differential scanning calorimetry was carried out in a Q1000 calorimeter from TA Instruments in nitrogene. The samples were crimped in the aluminum cell and subjected to two heating and cooling cycles at 10 °C/min from 0 to 150 °C followed by one cycle 0−280 °C and one cycle 0−400 °C. Elemental analysis was performed at the RXB Analytical Facility at the Materials and Manufacturing Directorate AFRL, WPAFB, OH.

**Functionalization of $TiO_2$ Nanoparticles with Phosphonic Acid.** Synthesis of 3-bromopropyl phosphonic acid (BPPA) (**1**, Scheme 1) was performed based on the previously reported procedure[18] and is described in detail in the Supporting Information. Reaction of titania with both BPPA and diethyl 3-bromopropane-1-phosphonate (DEBPP) was tested in different solvent systems, including water, toluene, methylene chloride, acetonitrile, and 1-butanol. The reaction with BPPA in toluene at 95 °C resulted in the highest degree of functionalization. For this procedure, 1 g of $TiO_2$ was dried in vacuum at 150 °C for 2 h and transferred into a 250 mL round-bottom flask, containing a solution of 150 mg of BPPA in 200 mL of dry toluene. The mixture was stirred by a high shear mixer for 60 min. A stir bar was added, the flask was closed with the septum and immersed into the oil bath at 95 °C, and the mixture

(15) Akcora, P.; Liu, H.; Kumar, S. K.; Moll, J.; Li, Y.; Benicewicz, B. C.; Schadler, L. S.; Acehan, D.; Panagiotopoulos, A. Z.; Pryamitsyn, V. *Nat. Mater.* **2009**, *8*, 354.
(16) White, M. A.; Maliakal, A.; Turro, N. J.; Koberstein, J. *Macromol. Rapid Commun.* **2008**, *29*, 1544.
(17) Ranjan, R.; Brittain, W. J. *Macromolecules* **2007**, *40*, 6217.
(18) Traina, C. A.; Schwartz, J. *Langmuir* **2007**, *23*, 9158.

**Scheme 1. Synthesis of the Azide-Functionalized Titanium Dioxide and Grafting of the Alkyne-Terminated Polystyrene**

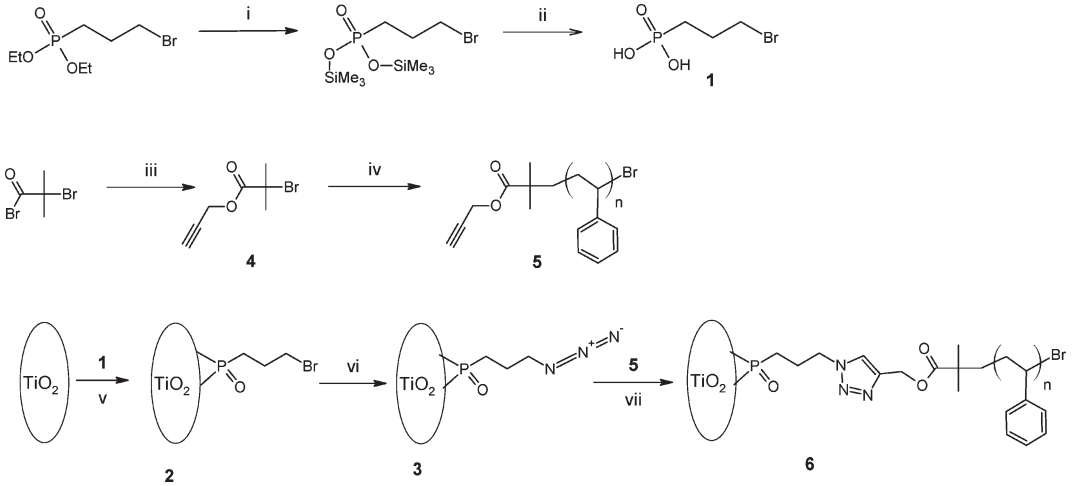


(i) $Me_3SiBr$, $CH_2Cl_2$, r.t., 48 h; (ii) $H_2O$/HCl; (iii) propargyl alcohol, pyridine, $Et_2O$, 0 °C, 24 h; (iv) styrene, CuBr/PMDETA, anisole, 90−110 °C. 2.5-33 h depending on M; (v) toluene, 95 °C, 16 h; (vi) $NaN_3$, DMF, 80 °C, 6 h; (vii) CuBr/PMDETA, toluene, 85 °C, 2−6 days depending on M of polystyrene.

was stirred for 15 h. At the end of the reaction, the flask was cooled to room temperature, and the solid was centrifuged at 6000 rpm (RCF = 3800 g) for 30 min, redispersed in 100 mL of methanol, centrifuged at 6000 rpm for 30 min, and dried in vacuum at room temperature for 24 h, yielding the phosphonic acid-functionalized nanoparticles **2**. A 100 mg sample of the material for NMR, FTIR, and elemental analysis was additionally washed successively by 50 mL of methanol, acetone, and diethyl ether by dispersion-centrifugation and dried in vacuum at room temperature until constant mass.

**Azide Modification of the Functionalized TiO2 Particles.** One gram of the phosphonic acid-functionalized nanoparticles **2** was mixed with 1 g of sodium azide in 100 mL of DMF by 60 min of high shear mixing in a 200 mL round-bottom flask. A stir bar was added, and the flask was closed with a septum, immersed into an oil bath at 80 °C, and stirred for the time ranging from 4 to 16 h. The flask was cooled to room temperature, and the mixture was centrifuged at 6000 rpm for 30 min. The solid was washed with water by 2 cycles of dispersion-centrifugation using 100 mL of water in each cycle, followed by drying in vacuum at room temperature until constant mass, yielding the azide-functionalized nanoparticles **3**.

**Synthesis of Polystyrene.** The synthesis of propargyl 2-bromo-2-methylpropanoate **4** was performed based on the published procedure,[19] which is reiterated in the Supporting Information. Samples of polystyrene **5** with $M_N$ 2800 g/mol PDI 1.07 (PS3k), 57,000 g/mol PDI 1.2 (PS60k), and 103,000 g/mol PDI 1.22 (PS100k), as determined by SEC, were synthesized by a typical CuBr-catalyzed atom transfer radical polymerization of styrene in anisole. The amounts of the monomer, solvent, initiator (CuBr), and ligand (PMDETA) as well as reaction time depended on the required molecular weight of polystyrene. These details can be found in the Supporting Information. The as-prepared PS100k was fractionated by the addition of methanol to the 50 g/L THF solution of the polymer until the solution turned opaque. This was followed by separation of the precipitated high molecular weight fraction by centrifugation at 6000 rpm. Molecular weight of the samples was determined by SEC. For the sample of PS3k the degree of polymerization was additionally determined by $^1H$ NMR in $CDCl_3$ by the ratio of the area under signals of aromatic protons of styrene and methyl protons on the terminal functionality.

**Grafting of Polystyrene to $TiO_2$ Nanoparticles.** For the grafting procedure, 1.5 g of polystyrene **5** was mixed with 1 g of the azide-midified $TiO_2$ **3** in 100 mL of toluene in a 200 mL round-bottom flask by high shear mixing for 30 min. The stir bar was added, and the flask was closed with the septum and purged with argon through the needle for 30 min. The flask was opened, 100 mg of CuBr and 100 $\mu$L of PMDETA were added, the septum was replaced, and purging continued for another 10 min. The needles were removed, and the flask was immersed in the oil bath at 85 °C and stirred for the time ranging from 24 h to 7 days in order to estimate the optimal reaction time. The highest degree of polymer grafting was achieved in 48 h for PS3k, 120 h for PS60k and 150 h for PS100k. For grafting of $TiO_2$ with a mixture of PS100k and PS3k 1 g of azide-modified $TiO_2$, 1 g of PS100k, and 0.5 g of PS3k were used, and the reaction time was 150 h. The reaction was stopped by cooling the flask to room temperature, and the mixture was homogenized by 30 min of high sheer mixing and centrifuged at 6000 rpm for 30 min. The precipitate was subjected to two more cycles of dispersion-centrifugation, the supernatants were combined, and the soluble fraction of the functionalized $TiO_2$ was separated from the free polymer by centrifugation at 200,000 g (45,000 rpm) for 2 h. The precipitate was redispersed in 180 mL of toluene (volume of 2 centrifuge tubes) and centrifuged one more time at the same conditions to ensure the complete removal of the free polymer. The final solid was dispersed in 50 mL of chloroform, precipitated into 200 mL of ethanol to remove residual CuBr, and dried in vacuum at 25 °C to constant mass. The insoluble fraction left after the first 3 cycles of dispersion-centrifugation was collected and dried at the same conditions.

**Cleavage of PS from Grafted Nanoparticles.** Polymer was cleaved by acidic hydrolysis according to the literature procedure.[20] A 50 mg sample was dispersed in 15 mL of 1,2-dichlorobenzene by stirring in a 50 mL round-bottom flask, 7 mL of 1-butanol and 0.5 mL of concentrated sulfuric acid were added, a reflux condenser was connected, and the flask was immersed in the oil bath at 95 °C and stirred for 6 days. The mixture was evaporated to 2 mL, dissolved in 20 mL of chloroform, and

(19) Luedtke, A. E.; Timberlake, J. W. *J. Org. Chem.* **1985**, *50*, 268.

(20) Qin, S.; Qin, D.; Ford, W. T.; Resasco, D. E.; Herrera, J. E. *Macromolecules* **2004**, *37*, 752.

extracted with 3 × 20 mL of water. The organic phase was evaporated, the dry residue was extracted with 2 mL of THF, and the solution was filtered through the 0.2 $\mu$m PTFE syringe filter and analyzed by SEC chromatography.

**Preparation of Assemblies of Hybrid Nanoparticles and Dielectric Characterization.** Free-standing films for TEM and X-ray spectroscopy were prepared by evaporation of the chlorobenzene solutions of the hybrid nanoparticles in a PTFE mold at ambient conditions. Dielectric measurements were made using thin films, fabricated in a class 1000 cleanroom environment. The hybrid nanoparticles were deposited on ITO glass substrates obtained from Colorado Concepts, from the 2.5% chlorobenzene solution by spin-coating at 900 rpm on a P 6700 Specialty Coating Systems spin coater. The films were either dried at 100 °C and 200 mbar for 24 h or annealed at 160 °C and 0.01 mbar for 48 h. To test the stability of the material at annealing, a 10 mg sample of the same material used for the film preparation was placed in the vacuum oven next to the thin film. The sample was extracted with 2 mL of THF, and the solution was filtered through the 0.2 $\mu$m PTFE syringe filter and analyzed by SEC chromatography. The thickness of the films was measured using a Tencor P-10 profilometer.

Subsequent to film deposition and heat treatment, Al electrodes, with a thickness of 100 nm ± 5 nm, were deposited on the top surface of the $TiO_2$ nanoparticle film using a BOC Auto 500 Thermal Evaporation System, to make a metal-insulator-ITO sandwich structure. Contact with the ITO was facilitated through the removal of the $TiO_2$ nanocomposite film adjacent to the top electrodes. In order to mitigate against the possibility of pinhole formation during electrical measurements by probe contact to the top surface, a guarded electrode structure was developed. Specific areas of the ITO layer were etched through a HCl treatment, prior to spin coating of the $TiO_2$ nanocomposite film. Al electrodes were deposited through a mask to include the etched areas, allowing for safe probe contact and the prevention of a short circuit. Schematics of the experimental setup are provided in the Supporting Information.

Impedance measurements were collected in the frequency domain using a NovoControl Alpha Impedance Analyzer, accompanied with a Novocontrol 4-wire Impedance Interface. Electrical contact was achieved by Au pin probes using a linear 4-probe measurement technique, in order to eliminate the deleterious effects of stray currents and lead inductance. Phase sensitive measurements of current and voltage were conducted (voltage/current = complex impedance, $Z^*$), and the resulting complex impedance and phase angle were converted and plotted as permittivity ($\varepsilon'$) and dielectric loss ($\varepsilon''$).

## Results and Discussion

**Functionalization of Titania Nanoparticles with Phosphonic Acid.** Scheme 1 outlines the synthesis of the polystyrene-grafted $TiO_2$ nanoparticles. The advantage of using the alkyne containing initiator vs postsubstitution of the terminal bromine with azide is that in the ATRP reaction practically every polymer molecule retains the initiator functionality, whereas the terminal bromine is gradually lost at higher conversions due to various termination pathways.[21] Moreover, monitoring of the substitution of bromine in a high molecular weight polymer (0.08% of Br in the $10^5$ g/mol polystyrene) is a difficult task. For the functionalization of nanoparticles, the bromopropyl moieties were introduced to the surface first, and substitution of bromine was performed afterward, in order to avoid the use of the potentially combustible 3-azidopropyl phosphonic acid.

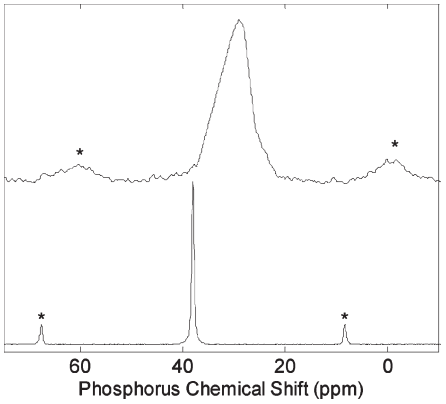


**Figure 1.** The solid-state 202 MHz cross-polarization magic-angle sample spinning phosphorus NMR spectra of (bottom) 3-bromopropyl phosphonic acid (38 ppm) and (top) modified titania particles (29 ppm). The spinning side bands are marked (*).

A sample of the industrial grade titanium dioxide was chosen with the aim of developing a potentially scalable synthetic procedure. The nanoparticles in the material were of a rodlike shape, 18 nm in diameter (by TEM and SAXS of solution) and 40−50 nm long (by TEM). Phosphonic acid derivatives have been shown to be versatile ligands suitable to a large variety of metal oxides, including $TiO_2$,[22,23] $Al_2O_3$,[23,24] $Y_2O_3$,[18] and $BaTiO_3$.[6] In contrast to silanes, binding of phosphates is not impaired by moisture or complicated by multilayer formation.[25] Reaction of titania nanoparticles with 3-bromopropyl phosphonic acid (BPPA) and its diethyl ester (DEBPP) was studied in various solvent systems including water, toluene, methylene chloride, acetonitrile, and 1-butanol. The first two solvents were chosen based on the literature procedure,[22] while other solvents were used due to their better ability to suspend $TiO_2$ particles. Figure 1 represents a typical $^{31}P$ solid-state NMR spectrum for the BPPA-functionalized sample. The broadening and downshift of the phosphorus peak in the functionalized nanoparticles from 38 to 29 ppm with respect to the spectrum of BPPA indicates covalent bonding of the phosphonic acid on the titania surface.[8,23]

Table 1 reports the degree of functionalization of the titania nanoparticles in various reaction conditions and solvents. Phosphonic acid generally yielded a higher degree of functionalization of $TiO_2$ particles than the corresponding diethyl ester. Among all the tested organic solvents toluene was the most effective despite the lowest solubility of BPPA in this solvent. Titania nanoparticles did not suspend in toluene and precipitated immediately

(21) Jakubowski, W.; Kirci-Denizli, B.; Gil, R. R.; Matyjaszewski, K. *Macromol. Chem. Phys.* **2008**, *209*, 32.
(22) Guerrero, G.; Mutin, P. H.; Vioux, A. *Chem. Mater.* **2001**, *13*, 4367.
(23) Gao, W.; Dickinson, L.; Grozinger, C.; Morin, F.; Reven, L. *Langmuir* **1996**, *12*, 6429.
(24) Guerrero, G.; Mutin, P. H.; Vioux, A. *J. Mater. Chem.* **2001**, *11*, 3161.
(25) Mutin, P. H.; Guerrero, G.; Vioux, A. *J. Mater. Chem.* **2005**, *15*, 3761.

**Table 1. Reaction Conditions and Degree of Functionalization of the TTO-51N $TiO_2$ Functionalized with Phosphonic Acid and Its Diethyl Ester**

| | reaction conditions | | | | |
|---|---|---|---|---|---|
| reagent | solvent | *T* (°C) | time (h) | P content, %, ±0.05 | degree of grafting, mmol/g $TiO_2$ |
| DEBPP | $CH_2Cl_2$ | 25 | 72 | 0.25 | 0.08 |
| | $C_4H_9OH$ | 100 | 24 | 0.3 | 0.1 |
| | $PhCH_3$ | 25 | 72 | 1.0 | 0.32 |
| | | 100 | 24 | 0.8 | 0.25 |
| BPPA | $CH_3CN$ | 25 | 72 | 0.9 | 0.3 |
| | $C_4H_9OH$ | 25 | 72 | 0.9 | 0.3 |
| | $PhCH_3$ | 25 | 72 | 1.1 | 0.35 |
| | | 100 | 24 | 1.1 | 0.35 |
| | $H_2O$ | 100 | 24 | 1.1 | 0.35 |

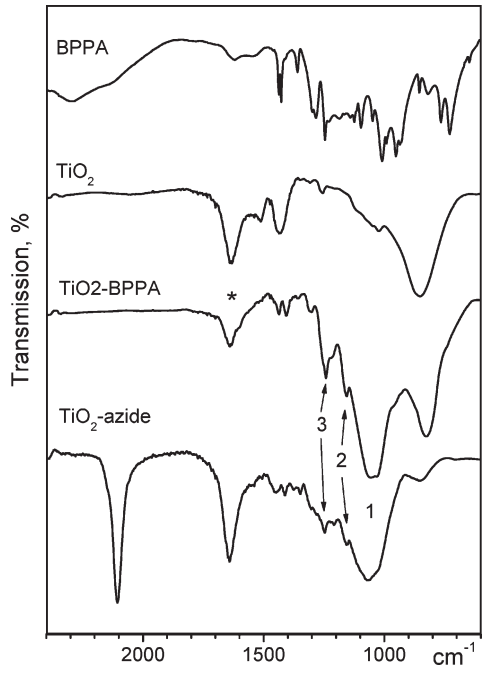


**Figure 2.** FTIR spectra of BPPA and $TiO_2$ in pristine form and after reaction with BPPA and sodium azide. The star denotes the 1640 $cm^{-1}$ peak from the Ti−O vibrations of $TiO_2$. Peaks 1, 2, and 3 correspond to P−O (1), P−C (2), and P═O (3) stretching vibrations of phosphonic acid in the spectra of $TiO_2$−BPPA and $TiO_2$−azide.

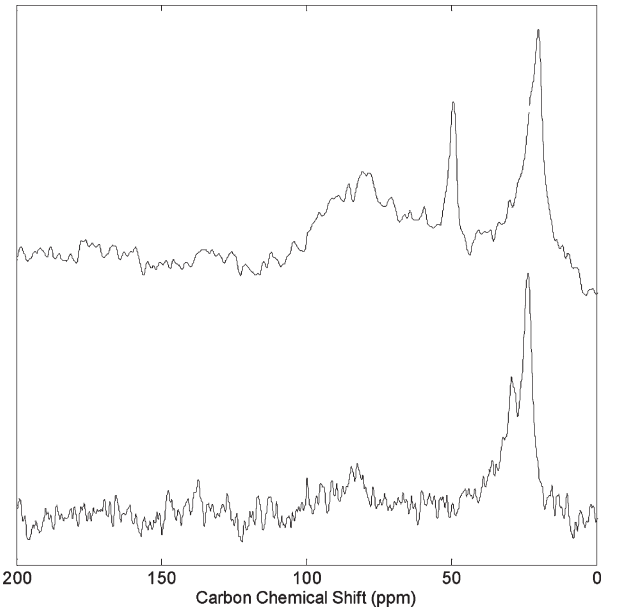


**Figure 3.** $^{13}C$ solid-state NMR of $TiO_2$−BPPA (bottom) and $TiO_2$−azide (top). The peak shifts are 20 ppm (−C−$CH_2$−), 29 ppm (−C−Br), and 49 ppm (−C−$N_3$).

after stirring or ultrasonication. However, addition of phosphonic acid followed by short high shear mixing stabilized the suspension. Reaction in the refluxed solvent normally required a shorter time to reach the highest possible degree of functionalization compared to the reaction at room temperature. At the monolayer coverage, each molecule of phosphonic acid occupies 0.24 $nm^2$ of the surface, as it was estimated by Gao and co-workers for 25 nm spherical particles.[23] Such a density corresponds to 0.38 mmol of ligand per 1 g of the 18 × 40 nm $TiO_2$ nanorods used in our experiments.

Phosphonic acid normally attaches to the surface of titanium dioxide by bi- and tridentate coupling, where the latter involves all 3 oxygens coordinated to the surface.[22] FTIR spectra of the BPPA-functionalized titania in Figure 2 reveals a broad peak at 1050 $cm^{-1}$ (denoted as #1), corresponding to the P−O stretching vibrations of the surface-bound phosphonic acid and a small peak at 1130 $cm^{-1}$ (#2) arising from P−C vibrations.[26] At the same time, a peak at 1236 $cm^{-1}$ (#3) from the P═O stretching vibrations of the unbound acid points out that some of the phosphoryl oxygens were not coordinated on the surface of $TiO_2$, thus suggesting a mixture of bi- and tridentate coupling.

**Synthesis of Azide-Functionalized Titania.** Azide functionalities were introduced to nanoparticles via nucleophilic substitution of bromine in the BPPA-modified material by reaction with sodium azide in DMF at 80 °C.[27] Substitution was confirmed by FTIR (Figure 2) and solid-state $^{13}C$ NMR (Figure 3). The new peak at 2100 $cm^{-1}$ in the FTIR spectra of the product in Figure 2 corresponds to the stretching vibrations of the azide groups.[17] In the $^{13}C$ NMR spectrum the peak at ∼29 ppm, corresponding to the −C−Br carbons, yields to the peak at 49 ppm, corresponding to the −C−$N_3$ carbons. The substitution procedure was complicated by hydrolysis of phosphonic acid from the titania surface in the presence of sodium azide, as suggested by reduction of phosphorus content with time (see Table 2). Heating of

(26) (a) Randon, J.; Blanc, P.; Paterson, R. *J. Membr. Sci.* **1995**, *98*, 119. (b) Persson, P.; Laiti, E.; Ohman, L.-O. *J. Colloid Interface Sci.* **1997**, *190*, 341.

(27) Carey, F. A.; Sundberg, R. J. *Advanced Organic Chemistry. Part B: Reactions and Synthesis*; Kluwer Academic: New York, 2001.

**Table 2. Elemental Analysis of the Phosphonate-Functionalized $TiO_2$ Treated with Sodium Azide**

| sample | element, functional group | content | |
|---|---|---|---|
| | | %, ±0.05 | mmol/g[a] |
| $TiO_2$−BPPA | P | 1.1 | 0.35 |
| | Br | 2.8 | 0.35 |
| $TiO_2$−BPPA in DMF 24 h, | P | 1.1 | 0.35 |
| | Br | 2.8 | 0.35 |
| $TiO_2$−BPPA + $NaN_3$ 4 h | P | 0.80 | 0.26 |
| | N, azide | 0.53 | 0.12 |
| $TiO_2$−BPPA + $NaN_3$ 6 h | P | 0.69 | 0.22 |
| | N, azide | 0.67 | 0.16 |
| $TiO_2$−BPPA + $NaN_3$ 16 h | P | 0.32 | 0.10 |
| | N, azide | 0.38 | 0.09 |
| TiO2-PS3k[b] | P | 0.61 | 0.22 |
| | N, azide+ triazol | 0.67 | 0.17 |

[a] Molar content by azide or/and triazol. [b] The $TiO_2$ content was 80 wt %.

the sample in DMF without $NaN_3$ for as long as 24 h did not change the content of phosphorus in the material, suggesting that the hydrolysis was facilitated by sodium azide. Our experiments conclude that the treatment with sodium azide for 6 h at 80 °C provides the best balance between the reaction yield (73% conversion) and loss of surface functionalities (63% of the ligand molecules retained on the surface).

**Grafting of Polystyrene by "Click" Coupling.** The copper-catalyzed Huisgen cycloaddition between azides of the $TiO_2$ surface and alkynes of the polystyrene allowed attachment of polymer molecules on nanoparticles. Although the polystyrene initially contained some residual Cu catalyst after the ATRP polymerization, it would have been oxidized during the workup procedure; therefore, the fresh catalyst was added to facilitate the cycloaddition. High air sensitivity of CuBr accounted for the fact that the samples prepared with no degassing had about 30% lower amount of the attached polymer, as estimated by TGA, compared to the samples degassed by purging with argon prior to the reaction. However, more thorough degas procedures, such as "freeze-pump-thaw", did not improve the efficiency of grafting. The optimal reaction time was estimated by performing several experiments with each sample by 24 h increment followed by TGA of the products. It was found that the highest grafting density of the polymer was achieved in 48 h for the 3k polystyrene, whereas the 100k material required 6 days to reach the maximum. In all the experiments, less than 20% of the polymer in the reaction mixture covalently attached to nanoparticles. Increasing the amount of 100k polystyrene by 3-fold did not increase the grafting density. This indicates that maximum grafting density was defined by size of the polymer chains and not by concentration of the reactants.

Polystyrene-grafted $TiO_2$ dispersed readily in toluene yielding milky suspensions stable for several days. The material was separated into "soluble" and "insoluble" fractions by means of centrifugation at 6000 rpm (ca. 3800 g) for 30 min, so that "solubility" here is arbitrarily defined as the ability of nanoparticles to withstand the said centrifugation conditions.

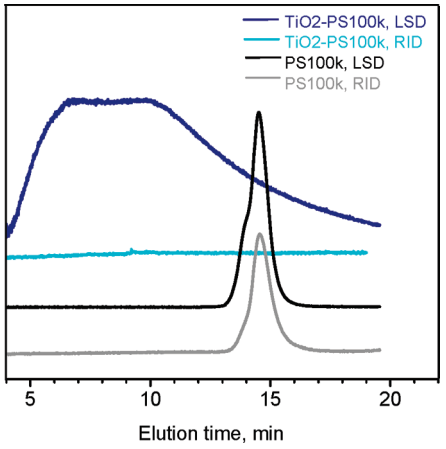


**Figure 4.** SEC chromatograms of the polystyrene PS 100k: light scattering at 90 deg (black) and refractive index (gray) signals, both showing a peak at 14.7 min. SEC chromatograms of the purified $TiO_2$ grafted with PS 100k: light scattering at 90 deg signal (dark blue) showing scattering from nanoparticles and refractive index signal (blue) showing absence of free polystyrene.

Absence of the free unattached polymer in the final purified materials was confirmed by size-exclusion chromatography. In Figure 4, the light scattering signal chromatogram of the 1 mg/mL solution of the purified TiO2-PS100k sample shows the broad peak arising from nanoparticles passing through the column, whereas the refractive index signal does not reveal a peak at 15 min, indicating no free polymer in the sample. Absence of the refractive index peak for nanoparticles can be explained by the fact that the material was eluted gradually over a long period of time without producing a fraction with the concentration sufficient enough for the detector. Therefore, the weight loss in TGA reported in Table 3 reflects only the amount of polystyrene chemically attached to nanoparticles, thus permitting estimation of the degree of grafting from this analysis. Chromatograms of the polymer cleaved from different samples of grafted nanoparticles in Figures 5 and 6 do not reveal a substantial difference in the weight-average molecular weight between the polystyrene used for functionalization and the one actually attached to the particles. However, the extended low molecular weight tail of the cleaved PS100k polymer suggests some higher reactivity of the smaller chains toward grafting to nanoparticles, which is explained below.

The mass balance of the grafting reaction in Table 3 shows that the yield of the functionalized nanoparticles increases with molecular weight of polystyrene. Thus, $TiO_2$ grafted with the 100k PS produced 0.32 g of the material vs 0.25 g in the $TiO_2$ grafted with 60k PS, despite nearly equal weight percent of the polymer in both samples. In the sample grafted with the mixture of 3k and 100k PS introduction of merely 9 chains of the 100k PS per particle doubled the amount of the functionalized $TiO_2$ compared to the sample grafted only with 3k PS. At the same time, the complete substitution of 3k PS with 100k PS for the synthesis produces over 5 times as much of the functionalized material. The yield of the grafted nanoparticles in this case is related to the purification

**Table 3. Characteristics of the Polystyrene Samples and Resulting Functionalized Materials**

| | sample | $TiO_2$-PS3k | $TiO_{i2}$-PS60k | $TiO_2$-PS100k | $TiO_{2T}$-PS100+3k |
|---|---|---|---|---|---|
| polystyrene | $M_W/M_N$, $\times 10^3$, g/mol | 3.2/2.9 | 68/57 | 125/103 | 125/103 + 3.2/2.9 |
| | Rg, nm[a] | 1.80 | 11.25 | 15.82 | 15.82 and 1.80 |
| | amount in the reaction mixture, g | 1.5 | 1.5 | 1.5 | 1.0 + 0.5 |
| $TiO_2$-azide | amount in the reaction mixture, g | 1.0 | 1.0 | 1.0 | 1.0 |
| | amount of azide groups, mmol/g | 0.16 | 0.16 | 0.16 | 0.16 |
| $TiO_2$-PS, soluble fraction | mass recovered, g, including: | 0.083 | 0.25 | 0.32 | 0.158 |
| | $TiO_2$, g (%) [b] | 0.07 (80.9%) | 0.18 (60.5%) | 0.22 (61.9%) | 0.13 (78.7%) |
| | $TiO_2$, particles [c] | $1.64*10^{15}$ | $4.21*10^{15}$ | $5.15*10^{15}$ | $3.04*10^{15}$ |
| | PS, g (%) [b] | 0.013 (19.1%) | 0.07 (38.5%) | 0.08 (38.1%) | 0.028 (21.3%) |
| | PS, chains | $2.45*10^{18}$ | $6.20*10^{17}$ | $4.01*10^{17}$ | $2.74*10^{16}+4.21*10^{18}$ [d] |
| | grafting density: chains/particle | 1494 | 147 | 78 | 9 + 1385 |
| | chains/$nm^2$ [c] | 0.54 | 0.05 | 0.03 | 0.50 (100k and 3k) |
| distance between grafting sites, nm[e] | | 1.36 | 4.34 | 5.96 | n/a |

[a] Rg was calculated for polystyrene chains in a good solvent by the formula provided in ref 29. [b] From TGA. [c] Considering each particle as a cylinder with $d = 18$ nm and $h = 40$ nm and density of 4.2 g/$cm^3$. [d] Relative amounts were estimated from SEC, using a relative area of the RID peaks. [e] Calculated by the formula: $D = 1/\sqrt{\sigma}$, where $\sigma$ is grafting density, in chains/$nm^2$.

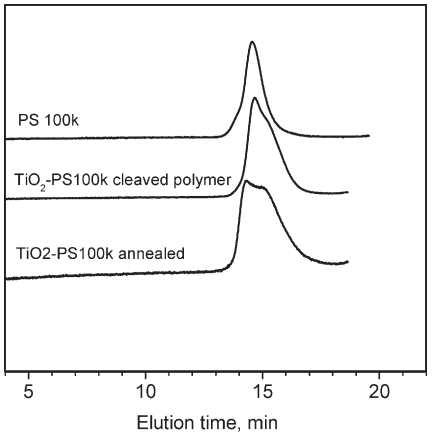


**Figure 5.** SEC chromatograms (refractive index signal) of the polystyrene PS 100k (top), polymer cleaved off the TiO2-PS100k (middle), and the THF extract of the same material annealed at 160 °C for 24 h (bottom).

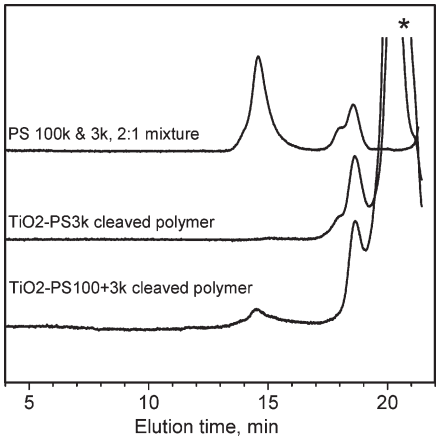


**Figure 6.** SEC chromatograms (refractive index) of the mixture of PS 100k and PS 3k, ratio of 2:1 by weight (top), polymer cleaved off the TiO2-PS3k (middle), and polymer cleaved off the TiO2-PS100 + 3k. The non-polymeric impurities extracted alone with cleaved polymers are marked (*).

procedure, in which only the particles that remained in the supernatant in centrifugation at 3800 g for 30 min were collected and analyzed. Longer polymer chains attached to the surface provided a better steric repulsion between the particles, resulting in a higher dispersibility and therefore a greater concentration of the functionalized material in solution after centrifugation.

The mass fraction of the attached polystyrene was calculated from the weight loss between 250 and 600 °C. Here, we ignored the contribution to the weight loss due to pyrolysis of azidoprolyl groups on the surface, which was 1.9% of the amount of $TiO_2$, based on the TGA of the $TiO_2$-azide. The number of nanoparticles in the samples was computed based on the approximate representation of the particles as cylinders with diameter of 18 nm and length of 40 nm, which was determined from TEM microscopy. The number of polymer chains in the sample was calculated by the formula $N = (m/M_W)*N_A$, where $m$ is the mass of the polymer part in the sample, $M_W$ is the weight average molecular weight, and $N_A$ is the Avogadro's number. The grafting density (in chains/$nm^2$) was calculated based on the surface area of 2771 $nm^2$ per particle. The average distance between grafting sites (in nm) was estimated by the formula $D = 1/\sqrt{\sigma}$, where $\sigma$ is grafting density (in chains/$nm^2$).

The "mushroom-to-brush transition" point of the polymer anchored on the surface is defined as the highest grafting density at which the chains are unperturbed.[28] The distance between grafting sites at such a point is equal to the size of the polymer coil or twice the radius of gyration $R_g$. Such a distance for the functionalized $TiO_2$ nanoparticles, estimated from the TGA results (Table 3), is lower than $2R_g$ for the corresponded polystyrene chains, which suggests that the polymer molecules attached to titania nanoparticles must be distorted and exist in the brush regime. Here, radius of gyration $R_g$ for polystyrene in a good solvent was calculated using the formula $R_g = (b/\sqrt{6})*(M_w/M_0)^{0.6}$, where $b$ is the length of the Kuhn segment (1.8 nm for polystyrene), $M_w$ is the weight average molecular weight, and $M_0$ is the molar mass of the Kuhn segment (720 g/mol for polystyrene).[29] It has been shown theoretically that anchoring of the end-functionalized polymer to the surface is limited not simply

(28) Iyer, K. S.; Zdyrko, B.; Malz, H.; Pionteck, J.; Luzinov, I. *Macromolecules* **2003**, *36*, 6519.

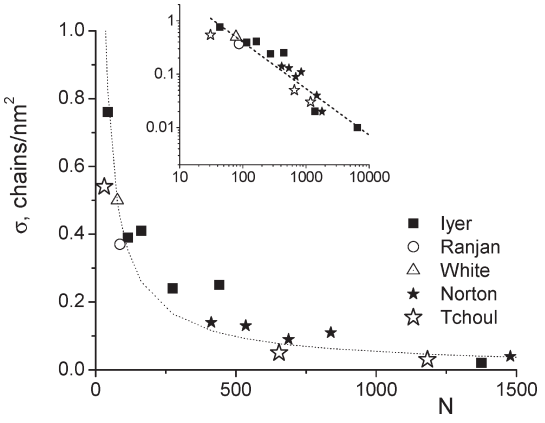


**Figure 7.** Grafted density as a function of a degree of polymerization for experimental and literature results. The data have been taken from refs 16 (White), 17 (Ranjan), 28 (Iyer), and 32 (Norton). The dotted line represents the best fit as $\sigma \sim N^{-0.87}$. Insert: data on the logarithmic scale.

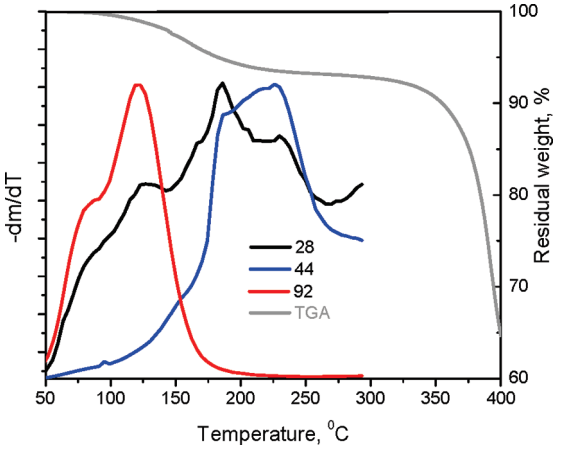


**Figure 8.** TGA-MS of the $TiO_2$−PS in helium, signals for selected mass ions: 28 amu ($N_2$, black), 44 amu ($CO_2$, blue), and 92 amu (toluene, red). Gray line corresponds to weight loss in TGA.

by size of molecules in solution but by the equilibrium between energy gain due to reaction of the end group of polymer with the surface of particles and entropic energy loss due to the chain constraint.[30,31] In consistence with this assumption, a number of publications report the brush formation in grafting of the end-functionalized polystyrene to the surface of silicon[28] and epoxy resin[32] as well as silica[17] and titania[16] nanoparticles. The plot in Figure 7 contains the compilation of the literature data along with our experimental results for the soluble fractions of TiO2-PS. Despite the differences in the substrates and grafting chemistry all the data fit reasonably well in the power law function $\sigma \sim N^{-\delta}$, where $0 < \delta < 1$, which was empirically proposed by Iyer et al.[28] This is especially illustrative if the numbers are plotted on the log scale (insert in Figure 7). The latter allows estimation of the coefficient $\delta = 0.87$.

**Particles with the Mixed Polymeric Corona.** The ratio of the grafted chains in the mixed corona particles of TiO2-PS100+3k was determined through hydrolysis of polystyrene off the surface of $TiO_2$ and analysis of the resulting mixture by chromatography. The chromatogram in Figure 6 shows that PS3k constituted the major portion of the hydrolyzed polymer. It overlapped with the peak from nonpolymeric products of hydrolysis, subtraction of which allowed an approximate estimation of the mass fractions of PS100k and PS3k as 20% and 80%, corresponding to the molar ratio of high and low $M_w$ components in the mixed corona of approximately 1:150. The initial ratio of PS100k and PS3k in the reaction mixture was 2:1 by weight or approximately 1:20 by mol. Theoretically, the shorter chains experience a much lower energy barrier to adsorption, as discussed by Milner.[33] Thus, a greater molar fraction of PS3k in the corona compared to that in the reaction mixture is anticipated. Here we again have to bear in mind that the determined values represent an average over the entire sample, which have a wide distribution of particles with different ratios of the grafted components.

**Stability of the Functionalized Nanoparticles.** The sample of TiO2-PS100k annealed at 160 °C in vacuum for 3 days was extracted with THF. The presence of the corresponding polystyrene was detected in the extract by chromatography (see Figure 5), suggesting the cleavage of polymer chains from particles at this temperature. To elaborate on this process, the material was heated up to 300 °C in helium, while the gaseous products were analyzed by mass spectrometry (Figure 8). Basically, two major groups of mass ions were detected. The first group evolved at 50−150 °C with a maximum at 120 °C and corresponded to distillation of residual solvents, primarily toluene (92 amu). The second group evolved at 150−250 °C and contained mass ions with 15−58 amu, presumably $CO_2$ (44 amu) and small hydrocarbons, corresponding to the products of decomposition of the linker between $TiO_2$ and polystyrene. Such decomposition, also confirmed by the endothermic peak in the DSC in Figure 13, explains cleavage of the polymer at 160 °C. The most characteristic signals from the two groups have been plotted in Figure 8: 92 (toluene molecular ion) and 44 amu (presumably $CO_2$ from ester groups). Nitrogen (28 amu) evolved constantly throughout the range with the highest intensity at 150−250 °C due to pyrolysis of azides and triazoles.[34] Decomposition of polystyrene in this sample started mostly after 350 °C, which is about 100 °C higher than that for the pure polymer.

**Matrix-Free Assembly of Hybrid $TiO_2$−PS Nanoparticles: Physical Properties.** The soluble fraction of the functionalized nanoparticles readily dissolved in a variety of organic solvents, where chlorobenzene was the best, producing yellowish opalescent solutions, which could be processed into 1−2 mm thick films by drop casting or into 100 nm thin films by spin coating. Recall, these films did

(29) Rubinstein, M. C.; Colby, R. H. *Polymer Physics*; Oxford University Press: New York, 2003.
(30) Netz, R. R.; Andelman, D. *Phys. Rep.* **2003**, *380*, 1.
(31) Ligoure, C.; Leibler, L. *J. Phys.* (*Paris*) **1990**, *51*, 1313.
(32) Norton, L. J.; Smiglova, V.; Pralle, M. U.; Hubenko, A.; Dai, K. H.; Kramer, E. J.; Hahn, S.; Berglund, C.; DeKoven, B. *Macromolecules* **1995**, *28*, 1999.
(33) Milner, S. T. *Macromolecules* **1992**, *25*, 5487.
(34) Huisgen, R.; Knorr, R.; Moebius, L.; Guenter, S. *Chem. Ber.* **1965**, *98*, 4014.

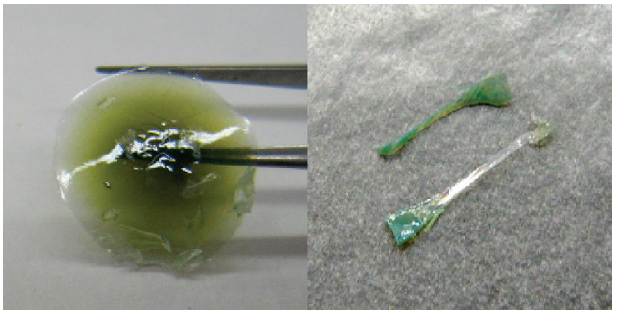

**Figure 9.** Left: A 2 mm thick film of the assembly of TiO2-PS100k hybrid nanoparticles obtained by evaporation of the toluene solution in the round-bottom tube. Right: the same film stretched after being heated above Tg.

not contain free matrix polymer but comprised solely of $TiO_2$ nanoparticles with a covalently grafted polystyrene corona. Despite a high inorganic content, 60−80% of titanium dioxide by weight, the films were optically transparent with a tint of green due to residual CuBr, as seen in Figure 9. The free-standing films made of TiO2-PS3k and TiO2-PS100+3k were too brittle to handle, while TiO2-PS60k and TiO2-PS100k were much more robust. In fact, it was possible to stretch the film of TiO2-PS100k by 2 times of the initial size by applying a tensile force to the sample suspended over the hot plate (Figure 9). Quantitative characterizations of the mechanical properties of the materials are ongoing. The TEM image of the drop-cast TiO2-PS100k film in Figure 10 shows uniform distribution of nanoparticles within the material. Moreover, such uniformity was confirmed by the differential Fourier transform analysis of this image (Figure 10), which correlated very well with the corresponding SAXS spectrum. The SAXS spectrum in Figure 11 features a well-pronounced peak for every sample, indicating a short-range packing of the particles. The average center-to-center distance $d$ between the particles can be estimated by the formula $d = 2\pi/q_{peak}$, giving the values of 26, 41, and 49 nm for the TiO2-PS3k, TiO2-PS60k, and TiO2-PS100k correspondingly. These values correlate with estimated end-to-end distance of the grafted polystyrene chains, suggesting the increased height of the brush on the surface of nanoparticles. There is no low $q$ upturn in any of the spectrum in Figure 12, indicating that there were no irregularities such as aggregated particles, agglomerates of the polymer, or nanosized pores. Absence of micrometer-size pores was confirmed by scanning electron microscopy (see the Supporting Information).

Figure 12 shows the differential scanning calorimetry results for the nanoparticles grafted with PS100k. The first two scans in the range of 0−150 °C were performed in order to erase the thermal history. In the third scan, a broad transition appears at ca. 60−80 °C. Residual toluene that was not completely removed during the drying, as indicated by the TGA-MS, acts as a plasticizer and most likely accounts for the reduction in glass transition temperature. An endothermic process occurred at the temperature range of ca. 140−230 °C, which has been explained above as decomposition of the linker between polymer and particle surface. In the next scan,

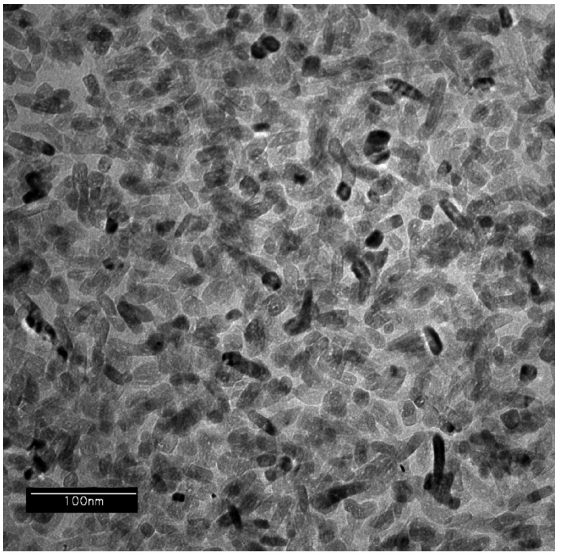


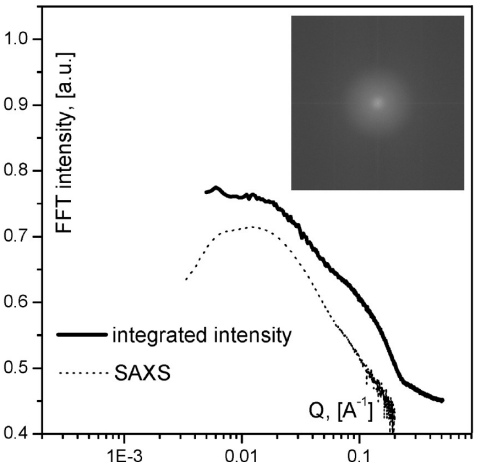


**Figure 10.** Top: TEM micrograph of a 75 nm thin section of the drop cast film of TiO2-PS100k. Bottom: DFT analysis of the TEM micrograph. Insert − FFT image. Solid line − integrated azimuthal intensity of FFT. Dotted line − SAXS for the same sample.

the glass transition of polystyrene manifested at 110 °C, which was a 5 °C increase compared to the $T_g$ of the sample of pure PS100k, in agreement with prior reports on glass transition of the tethered polymer chains.[35,36] Since some of the polymer was cleaved from the particles in the previous scan, the observed transition corresponds to the $T_g$ of both grafted and free polystyrene chains in the composite. The increase in the $T_g$ in the mixture of polystyrene-grafted silica nanoparticles and free polymer has been observed and described by Bansal et al.[37,38]

**Dielectric Spectroscopy of the TiO2-PS100k Thin Films.** Figure 13 represents the values of dielectric constant

(35) Tate, R. S.; Fryer, D. S.; Pasqualini, S.; Montague, M. F.; de Pablo, J. J.; Nealey, P. F. *J. Chem. Phys.* **2001**, *115*, 9982.
(36) Oyerokun, F. T.; Schweizer, K. S. *J. Chem. Phys.* **2005**, *123*, 224901.
(37) Bansal, A.; Yang, H. C.; Li, C. Z.; Cho, K. W.; Benicewicz, B. C.; Kumar, S. K.; Schadler, L. S. *Nat. Mater.* **2005**, *4*, 693.
(38) Bansal, A.; Yang, H.; Li, C.; Benicewicz, B. C.; Kumar, S. K.; Schadler, L. S. *J. Polym. Sci., Part B* **2006**, *44*, 2944.

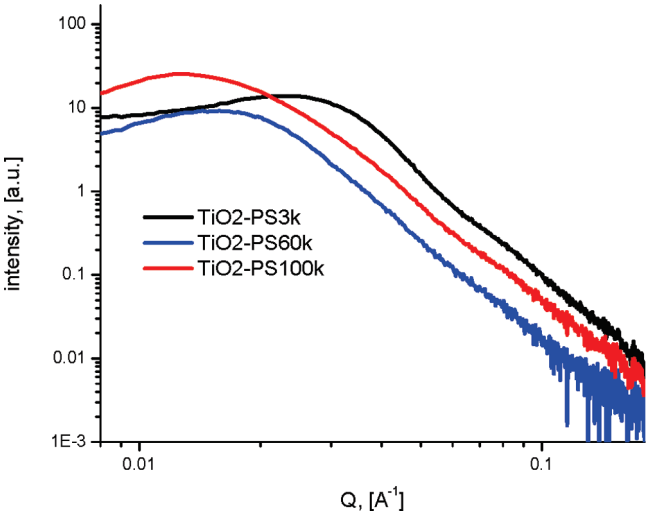


**Figure 11.** Small angle X-ray scattering of the TiO2-PS drop-cast films.

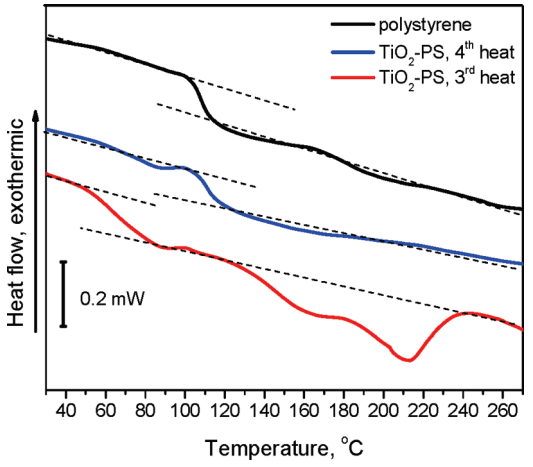


**Figure 12.** Differential scanning calorimetry of the TiO2-PS100k hybrid material and the corresponding 100k g/mol polystyrene.

and dielectric loss as functions of frequency for $TiO_2$−PS100k and the corresponding polystyrene sample. The "as prepared" sample of hybrid nanoparticles containing 27 vol % of $TiO_2$ was dried after deposition at 100 °C and 200 mbar to evaporate residual solvent. The dielectric constant $\varepsilon$' at 1 kHz for this sample was 6.4 compared to 2.7 for the film of PS100k polystyrene. The upturn of the dielectric constant of the "as-prepared" sample at low frequencies combined with the tremendous dielectric loss suggests the leakage of current in the sample presumably due to ionic conductivity. The material contained residual CuBr, which was used as a catalyst in "click" coupling reaction. This impurity resisted solvent extraction and purification due to being strongly bound to particles by complexation to azide and triazole functionalities. It is possible that $Br^-$ ions contributed to conductivity at low frequency, especially if traces of solvent remained in the material. Annealing of the film at 160 °C resulted in decomposition of azide and triazole moieties as well as in the complete solvent removal as TGA and DSC data indicate, thus preventing the mobility of bromide ions. Respectively, the low frequency current leakage was significantly reduced, as judged by the low value of the dielectric

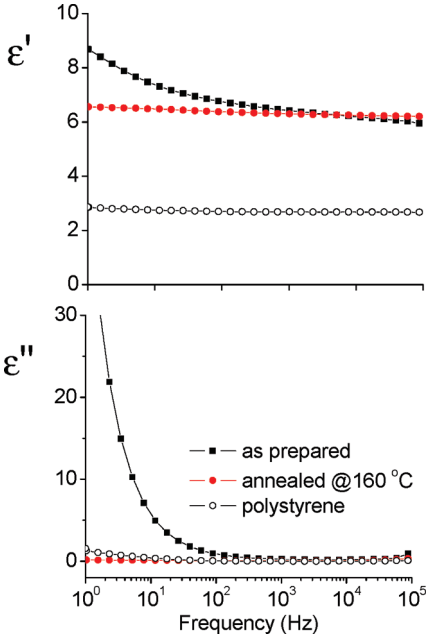


**Figure 13.** Dielectric spectroscopy of the thin film of TiO2-PS100k and PS100k polystyrene. Top: dielectric permittivity vs frequency; bottom: dielectric loss vs frequency.

loss ($\varepsilon$" = 0.04 at 1 kHz), which was practically unchanged over the whole spectrum. The breakdown strength experiments for this material are currently underway.

## Conclusions

The present work has demonstrated a versatile route for construction of a nanocomposite by direct assembly of hybrid core−shell nanoparticles without the use of the matrix polymer. Such a route enables a highly uniform distribution of particles and allows a precise control over the structure and interface and good processability. Titania nanoparticles grafted with the $10^5$ g/mol polystyrene were suitable for preparation of films of various thickness by solution casting or spin-coating. Despite containing 60 wt % of inorganic fraction, this material was mechanically robust and exhibited increased elasticity above the glass transition temperature, which indicates its potential suitability for compression molding or sheet extrusion.

The grafting density of polystyrene attached to the particles scales inversely with the molecular weight through a power law. The obtained values for the grafting density correlated closely with the literature data for grafting of the end-functionalized polystyrene to both flat surfaces and colloidal particles, indicating that the "grafting-to" approach is well controlled and predictable. Furthermore, grafting of the mixture of long and short polystyrene chains to the particles revealed a preferential attachment of the shorter chains, which complied with theoretical prediction. Dispersibility of the functionalized particles increased with molecular weight of the grafted polymer, owning to a stronger steric repulsion of the long chains. For example, the mixed corona sample having the molar ratio of the long and short chains of 1:20 produced twice as much of the soluble nanoparticles compared to

the sample grafted only with the short chains, while the weight fraction of the polymer in both samples was almost identical.

Thermal analysis of the material has shown that the linker between particles and polystyrene, containing ester and triazole groups, is susceptible to decomposition at the temperature range of 150−250 °C, which results in cleavage of the polymer from particles. Finally, the initial dielectric spectroscopy data imply that the complex permittivity of the nanoparticles assemblies depends not only on the content of the inorganic fraction but also on the structure and interfacial chemistry of hybrid particles. Therefore, the future research will focus on understanding of the impact of the nanoparticle surface chemistry and structure on these properties. Overall, matrix-free polymer-inorganic hybrid materials offer many intriguing possibilities for applications as diverse as structural elements to capacitors.

**Acknowledgment.** The authors thank Aurora Rubel from the Center for Applied Energy Research, University of Kentucky, Lexington, KY for the TGA-MS analysis, Marlene Houtz from AFRL/RXBN, WPAFB, OH for the TGA and DSC analysis, and Aaron Sellinger from AFRL/RXBN, WPAFB, OH for the atomic force microscopy. This research was performed while M. Tchoul, S. Fillery, and F. Oyerokun held the National Research Council Associateship Awards at AFRL. Funding for this project was available from the Air Force Office for Scientific Research.

**Supporting Information Available:** Synthetic procedures for all the compounds; GPC chromatograms for the polystyrene samples; $^1$H NMR spectra for the PS 3k polystyrene sample; WAXS spectrum for the $TiO_2$ nanoparticles; AFM micrographs; additional SEM and TEM micrographs; and schematics of the experimental setup for the dielectric spectroscopy. This material is available free of charge via the Internet at http://pubs.acs.org.